Lab on a Chip

Accepted Manuscript

ROYAL SOCIETY OF CHEMISTRY

www.rsc.org/loc

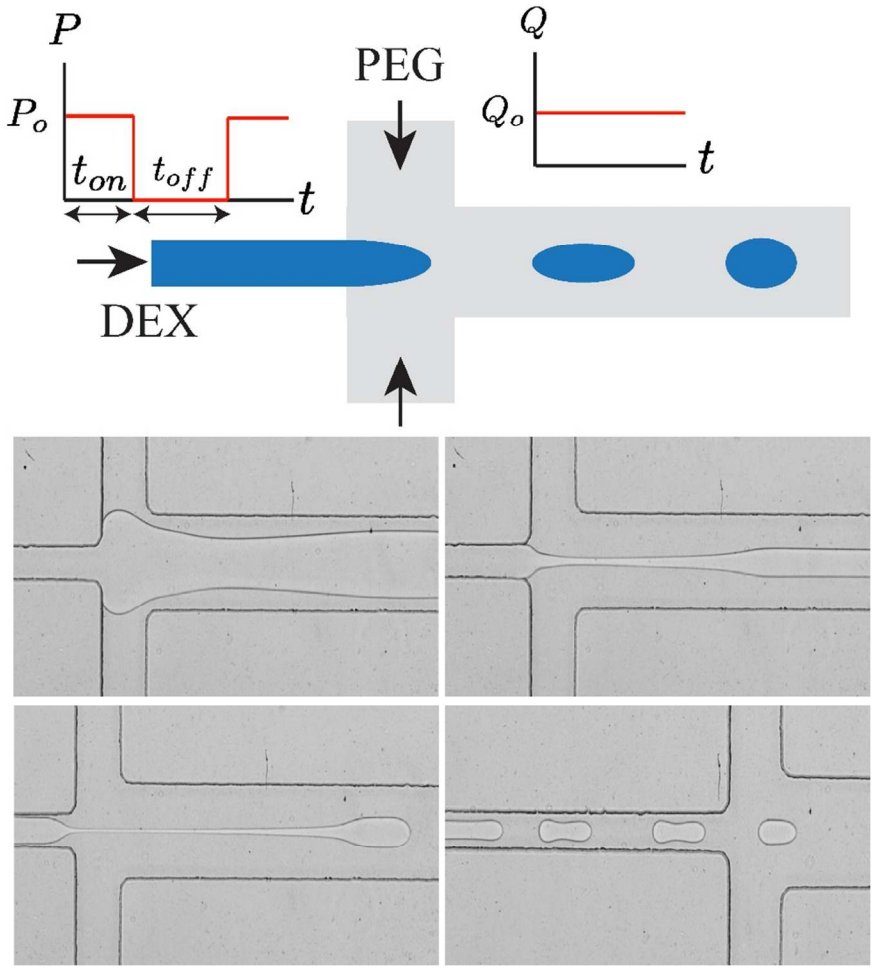

Simple microfluidic flow focusing generation of droplets from ultralow interfacial tension aqueous two phase systems (ATPS).

ARTICLE TYPE
www. rsc.org/xxxxxx | XXXXXXXX

Microfluidic generation of aqueous two-phase system (ATPS) droplets by controlled pulsating inlet pressures†

Byeong-Ui Moon,[a] Steven G. Jones,[a] Dae Kun Hwang,*[b] and Scott S. H. Tsai*[a]

Received Xth XXXXXXXXXX 20XX, Accepted Xth XXXXXXXXX 20XX
First published on the web Xth XXXXXXXXXX 200X
DOI: 10.1039/b000000x

We present a technique that generates droplets using ultralow interfacial tension aqueous two-phase systems (ATPS). Our method combines a classical microfluidic flow focusing geometry with precisely controlled pulsating inlet pressure, to form monodisperse ATPS droplets. The dextran (DEX) disperse phase enters through the central inlet with variable on-off pressure cycles controlled by a pneumatic solenoid valve. The continuous phase polyethylene glycol (PEG) solution enters the flow focusing junction through the cross channels at a fixed flow rate. The on-off cycles of the applied pressure, combined with the fixed flow rate cross flow, make it possible for the ATPS jet to break up into droplets. We observe different droplet formation regimes with changes in the applied pressure magnitude and timing, and the continuous phase flow rate. We also develop a scaling model to predict the size of the generated droplets, and the experimental results show a good quantitative agreement with our scaling model. Additionally, we demonstrate the potential for scaling-up of the droplet production rate, with a simultaneous two-droplet generating geometry. We anticipate that this simple and precise approach to making ATPS droplets will find utility in biological applications where the all-biocompatibility of ATPS is desirable.

1 Introduction

Aqueous two-phase systems (ATPS) are formed by the mixture of incompatible polymer solutions, most commonly polyethylene glycol (PEG) and dextran (DEX).[1,2] Above a critical polymer concentration, the mixture separates into two distinct aqueous phases, the lower density PEG-rich phase and the higher density DEX-rich phase.[3,4] The phase separation of ATPS is excellent for applications in protein separation and extraction,[5,6] cell partitioning,[7–9] bacterial and cell micropatterning,[10,11] and DNA extraction.[12,13] As a result of their biocompatibility and selectivity, equilibrated ATPS phases are also useful for biological applications that require multiple fluid phases.

In microfluidics, oil-water two-phase systems have been widely used to produce discrete monodisperse droplets.[14–17] These systems typically employ hydrodynamically-controlled flow focusing geometries to generate droplets, by exploiting the Rayleigh-Plateau instability of a central liquid jet within a continuous outer phase fluid (either water-in-oil or oil-in-water). Due to the relatively high interfacial tension (typical oil-water systems have interfacial tension $\gamma = 1 - 20$ mN m^{-1}), the liquid jet breaks up into small monodisperse droplets. The produced droplets vary in size from pico to nanoliters, and are used in reaction applications,[14] particle synthesis,[18] high-throughput assays,[19] and single cell analysis.[20] However, to use these droplets in biological applications requires extensive post-processing due to the toxic nature of the oil phase.[21]

ATPS was recently introduced into microfluidic devices, and already demonstrates the benefits of their biocompatibility, namely, in separating cells and proteins in a continuous manner,[22,23] in encapsulating cells,[24] and in biomolecule delivery.[9] However, due to the ultralow interfacial tension of ATPS (typically $\gamma = 0.1 - 100$ μN m^{-1}),[25,26] most ATPS microfluidics experiments have been limited to the manipulation of simple laminar flows. The ultralow interfacial tension of ATPS makes drop breakup in microchannels by the classical Rayleigh-Plateau instability difficult to achieve.[27]

As a result, microfluidic ATPS droplet generation relies on application of external forcing. For example, microfluidic ATPS droplet generation is possible by electrohydrodynamic perturbation of the ATPS interface at a T-junction.[28,29] Squeezing an ATPS jet to cause its breakup into droplets is possible with mechanical forcing from an oscillating piezoelectric disk, embedded next to a microchannel.[30,31] Lai et al.[32] also show monodisperse ATPS droplet formation with pin actuation in a rounded multi-level microchannel. Additionally, ATPS droplets and double emulsions can be achieved in glass capillary microfluidic devices, through controlled mechanical vibration of the flexible tubing that is connected to the inner stream of the capillary.[33–35]

Despite these approaches, generating ATPS droplets in microfluidics remains challenging. Namely, none of the existing methods are based on direct control of the flow into the microchannel. Consequently, there does not appear to be a

simple way to modify the channel designs such that many monodisperse droplets are produced at once.

Here, we present a simple, hydrodynamically-controlled system, for ATPS droplet generation in polydimethylsiloxane (PDMS) based microfluidic channels. We modulate the hydrodynamics by combining fluid inlets of oscillating pressure and constant flow rate. The disperse phase is injected into the inner channel with a pulsating applied pressure that is controlled by a solenoid valve, and the continuous phase enters the cross-flow inlet via a constant flow rate syringe pump. We experimentally obtain different drop formation regimes, and tune the resulting droplet size as we vary the magnitude and the 'on' and 'off' times of the applied pressure, and the continuous phase flow rate. We also develop a simple scaling model to predict the ATPS droplet sizes, and we find a good agreement with the experimental results. Finally, we demonstrate the potential scale-up of our ATPS droplet generation approach, by simultaneously forming double droplets with a single pressure source in a single microchannel.

The uniqueness of our approach lies in its simplicity: we use a conventional flow-focusing PDMS-glass microfluidic device without any additional components, and the square-wave pulsating pressure that we apply can be easily replicated by a commercially available pressure-controlled syringe pump (for example, the Fluigent MFCS-EZ). We anticipate that this simple technique will help to democratize microfluidic generation of monodisperse ATPS droplets.

2 Experimental methods

2.1 Chemicals

We phase-separate an aqueous solution containing 10 % (w/v) polyethylene glycol (PEG, Mw 8,000, Sigma-Aldrich, St. Louis, MI, USA) and 5 % (w/v) dextran (DEX, Mw 100,000, Sigma-Aldrich, St. Louis, MI, USA) for 24 hours, into the upper PEG-rich phase and the lower DEX-rich phase. Once equilibrated, we use syringes to isolate the two phases. We use a glass viscometer to measure the PEG-rich phase and DEX-rich phase viscosities $\mu_P = 8.7$ mPa s and $\mu_D = 99.8$ mPa s, respectively, and we use reports in the literature to estimate their ultralow interfacial tension $\gamma = O(10-100)\ \mu$N m^{-1}.[36,37]

2.2 Device fabrication

The microfluidic device is fabricated using standard soft lithography methods.[38] We draw the flow focusing channel geometry with computer-aided design (CAD) software (AutoCAD 2010, Autodesk, Inc., Dan Rafael, CA, USA) and print onto a transparency sheet (25,400 dpi, CAD/ART Services Inc., Bandon, OR, USA) to make the photomask. We spin-coat SU-8 2035 photoresist (Microchem., Newton, MA USA)

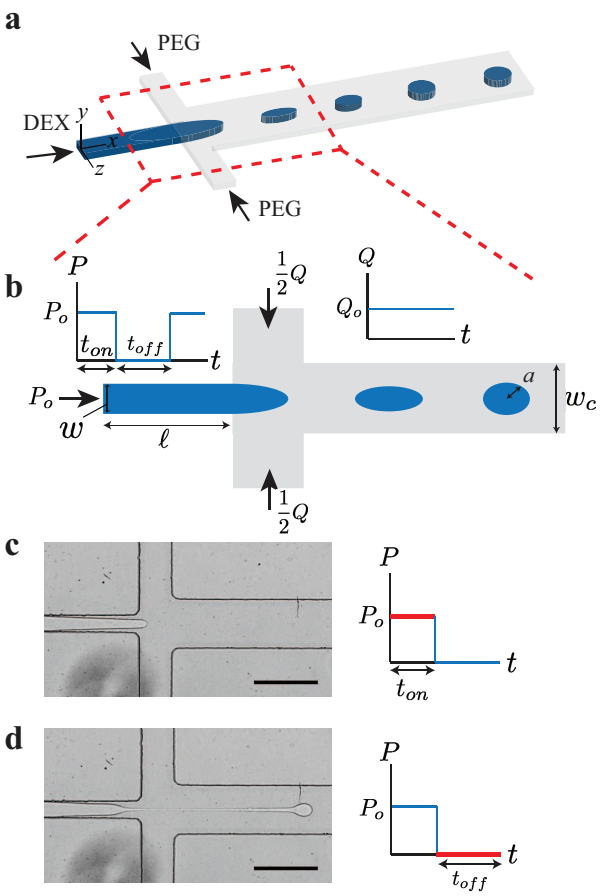

Fig. 1 (Color online) (a) Schematic diagram of ATPS droplet formation in a flow-focusing geometry. The DEX solution is injected by an applied pressure and the PEG solution is introduced by a syringe pump. (b) Droplet formation mechanism. A solenoid valve controls the on-off cycle of the applied pressure of the DEX inlet, and the PEG is introduced at a constant flow rate. When the inlet pressure is applied, (c) the pressure pushes the DEX solution into the cross-junction. With the inlet pressure off, (d) the DEX solution breaks into drops by the constant flow rate of the PEG sheath flow. Scale bar 200 μm.

onto a 4 inch silicon wafer (University Water Inc., Boston, MA, USA) and then expose the wafer to a UV light through the transparency photomask. After chemical development, the desired microchannel pattern is formed on the silicon master.

To make PDMS-glass bonded channels, we pour a 10:1 ratio mixture of PDMS resin and curing agent (Sylgard 184, Dow-Corning, Midland, MI, USA) onto the prepared silicon master, and cure it in an oven for 2 hours. A biopsy punch (Integra Miltex, Inc., Rietheim-Weilheim, Germany) is used to create inlet and outlet holes in the PDMS layer. We clean the PDMS sheet and a cover glass slide (Corning microscope slides 75 $\times$ 25 mm, Sigma-Aldrich, St. Louis, MI, USA) by sonication in ethanol, and dry both with nitrogen gas. After oxygen plasma treatment (Harrick Plasma, Ithaca, NY, USA), we bond the PDMS layer and glass slide irreversibly.

2.3 Experiment setup

ATPS droplets are generated by incorporating pulsating applied pressure and constant flow rates at the system inlets (Fig. 1 (a)). We load the DEX solution into a 250 μL pipette tip, and vertically insert the tip into the inner stream inlet of the microfluidic device. A Tygon tubing (Saint-Gobian, La Défense, Courbevoie, France) is interfaced with the other end of the pipette tip, and is used to transport compressed air to the DEX solution, to inject the solution into the microchannel (see schematic map in Supplementary Information Fig. S1).

In Fig. 1 (b), the DEX channel and downstream channel widths, $w = 50$ μm and $w_c = 150$ μm, respectively. The DEX channel length $\ell = 5$ mm, from the DEX inlet to the flow focusing junction. All microchannels have height, $h = 50$ μm.

A pressure regulator (Type 100LR, Control Air Inc., Amherst, NH, USA) is serially connected to a three-way solenoid valve (Model 6014, Burkert, Germany), to continuously tune the on-off cycles of the compressed air. The solenoid valve has a response time 10 - 20 ms. This setup is similar to experimental systems used in stop-flow lithography.[39] We control the valve by a customized LabVIEW (National Instruments, Austin, Texas, USA) program, and apply 'on' DEX inlet pressures P_o = 21 or 42 kPa. The PEG cross-flow is supplied via a constant flow rate syringe pump at flow rates $Q_o = 1$ or 3 μL min^{-1} (Harvard Apparatus, Holliston, MA, USA).

Experimental images of ATPS droplets are captured using an inverted microscope (Axio Observer.A1, Zeiss, Oberkochen, Germany) with an attached high speed camera (Vision Research, Wayne, NJ, USA). The high speed camera operates at a frame rate of 500 fps and an exposure time of 1,000 μs. We use ImageJ software to post-process the images and measure the size of droplets.

3 Results and discussions

3.1 Making ATPS droplets

We produce ATPS droplets in a flow focusing geometry, by application of a pulsating applied pressure to the disperse phase inlet, and a constant flow rate to the continuous phase inlet. Fig. 1 (b) shows that the disperse DEX solution pressure P switches between 'on', $P = P_o$, and 'off', $P = 0$. The corresponding 'on' and 'off' times are t_{on} and t_{off}, respectively. The continuous phase PEG is introduced at a constant flow rate, $Q = Q_o$, and enters via a single inlet which subsequently splits into the two sides of the cross flow at the flow focusing junction (Fig. 1 (b)).

During the pressure on-time t_{on}, the applied pressure pushes the DEX phase into the junction (Fig. 1 (c)). Then when the applied pressure is 'off', the constant flow rate of the continuous PEG phase shears a droplet off the DEX jet (Fig. 1 (d)). This continued on-off modulation of the applied pressure to the DEX phase, coupled with a constant flow rate of the outer PEG phase, enables generation of a steady stream of monodisperse DEX droplets.

Such ATPS droplet formation would not be possible with conventional droplet-making microfluidic flow focusing systems that apply constant flow rates for the disperse and continuous phases. Using a conventional setup with an ultralow interfacial tension ATPS, would result in a long and steady jet of the disperse phase, which, in the absence of external forcing, will not break into droplets within the length of the microchannel (see for example Supplementary Information Fig. S2).

3.2 Different regimes of ATPS interfacial dynamics

To investigate the behavior of the ATPS interface at the flow focusing junction, we fix the DEX 'on' pressure P_o and the PEG constant flow rate Q_o, and sweep across a range of DEX pressure 'on' and 'off' times, t_{on} and t_{off}, respectively. Fig. 2 (a) shows the phase diagram we obtain for the ATPS interfacial dynamics at the junction of the microchannel system. Here, the DEX 'on' pressure $P_o = 21$ kPa, and the PEG outer flow rate $Q_o = 1$ μL min^{-1}. We observe that the range of DEX pressure off-time t_{off}, that permits droplet generation (solid and empty diamonds), grows with increasing DEX pressure on-time t_{on}.

As shown in Fig. 2 (a) and (b), a small DEX pressure 'off' time, $t_{off} < 100$ ms, results in wide DEX jets that have a large wavelength interfacial perturbation (see top-left image in Fig. 2 (b), and Supplementary Information Movie 1). This deformation of the interface decreases downstream as the DEX-PEG interface stabilizes. A similar behavior occurs at a higher DEX pressure 'off' time, $100 < t_{off} < 300$ ms, where the

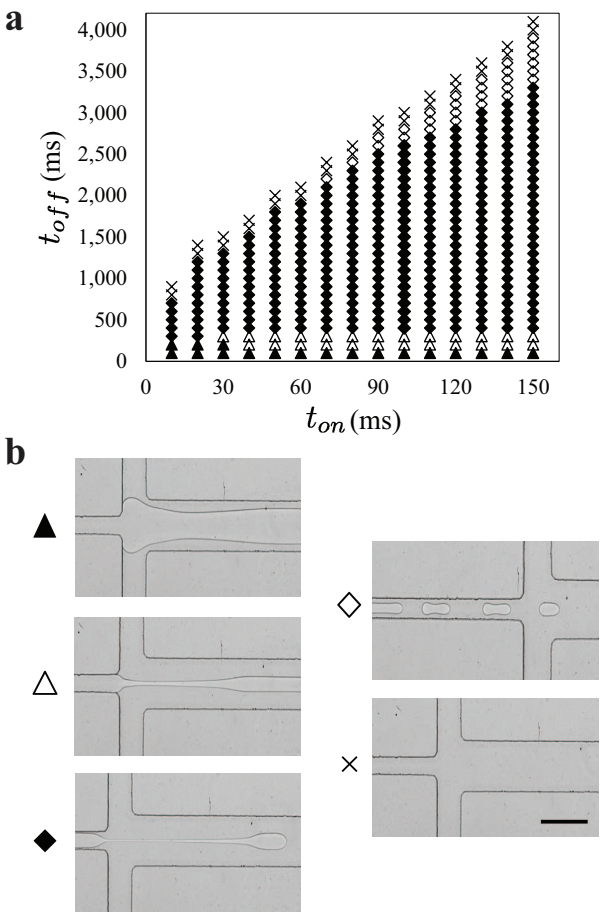

Fig. 2 (a) Phase diagram of ATPS interfacial dynamics in our microchannel. For this phase diagram, the inner DEX stream 'on' pressure $P_o = 21$ kPa and the outer PEG flow rate $Q_o = 1$ μL min^{-1}. We sweep across a range of pressure-on and pressure-off times, t_{on} and t_{off}, respectively, to investigate the resulting dynamics. Solid and empty diamonds correspond to regimes that allow for ATPS droplet formation. (b) Representative images of flow patterns observed in the microchannel: wide jets (solid triangles), narrow jets (empty triangles), downstream droplet formation (solid diamonds), upstream droplet formation (empty diamonds), and DEX phase backflow (crosses). Scale bar 200 μm.

DEX jet is more narrow and attains a similar interfacial perturbation (see middle-left image in Fig. 2 (b), and Supplementary Information Movie 2). In these two regimes, the shear stress from the PEG sheath flow is insufficient to completely break up the DEX jet into droplets.

Further increase of DEX pressure off-time, $t_{off} > 300$ ms, causes the PEG sheath flow to push the DEX jet into a neck (solid diamonds in Fig. 2 (a) and (b)). Eventually, the neck ruptures and a drop is formed upstream of the neck (see Supplementary Information Movie 3). This droplet generation regime is observed throughout a wide range of DEX pressure on-time and off-time values, t_{on} and t_{off}, respectively. We note that in this regime, trailing secondary drops are observed, and these drops follow the main droplet along the downstream channel.

Interestingly, we find a second droplet generation regime (empty diamonds) that is visually distinct from the previous regime (solid diamonds). Namely, at higher values of DEX pressure off-time t_{off}, we observe that small droplets are formed in the DEX channel that is upstream of the flow focusing junction (top-right image in Fig. 2 (b)). In this regime, the extended period of zero pressure in the DEX inlet causes a backflow of the disperse DEX phase and the continuous PEG phase into the upstream channel. The pull-back of the DEX jet also results in the formation of a neck in the upstream channel, which subsequently ruptures to form a DEX drop (see Supplementary Information Movie 4). The DEX droplet gets pushed into the flow focusing junction when the DEX inlet pressure is finally 'on'.

At even higher values of pressure 'off' time t_{off}, none of the DEX phase enters the cross-junction. Therefore, no droplets are generated in this regime (crosses in Fig 2 (a) and bottom-right image of Fig. 2 (b)).

We also study how the droplet formation regimes change with the value of the DEX phase applied pressure P_o, and the PEG phase flow rate Q_o. Fig. 3 shows a phase diagram with four DEX and PEG inlet combinations. Namely, the DEX phase 'on' pressure $P_o = 21$ or 42 kPa, and the PEG phase flow rate $Q_o = 1$ or 3 μL min^{-1}.

Across a range of pressure 'on' and 'off' times, t_{on} and t_{off}, respectively, we find that the drop-making regime expands with increasing disperse phase applied pressure P_o and decreasing continuous phase flow rate Q_o. This result is mainly due to the backflow of the DEX phase at higher values of the DEX pressure 'off' time t_{off}. At higher DEX phase applied pressure P_o, the pressure 'off' time t_{off} can be longer without causing DEX phase backflow into the upstream channel. Lowering the continuous PEG phase flow rate Q_o also helps to prevent backflow of the DEX phase. Therefore, the combination that achieves the largest droplet formation range is at a high DEX applied pressure $P_o = 42$ kPa and a low PEG flow rate $Q_o = 1$ μL min^{-1}.

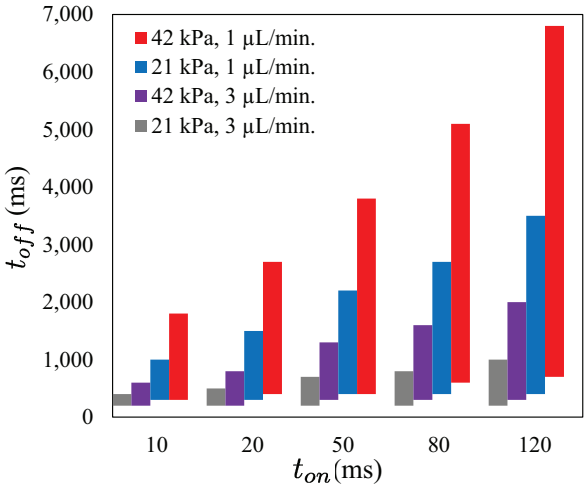

Fig. 3 (Color online) Phase diagram of regimes that permit droplet generation. Here, we apply DEX 'on' pressures $P_o = 21$ or 42 kPa and PEG flow rates $Q_o = 1$ or 3 μL min^{-1}, and sweep across a range of DEX pressure 'on' and 'off' times, t_{on} and t_{off}.

3.3 Elongated ATPS droplet shapes

In our system, the ultralow ATPS interfacial tension ($\gamma = O(10)$ μN m^{-1}) results in a large capillary number $Ca = \mu_P U/\gamma > 1$, provided that the DEX applied pressure is 'on' and produces an average flow speed U. As a result of the dominance of shear stress over interfacial tension, we observe that as the DEX droplets move downstream in the channel, they form an elongated shape (Fig. 4 (a)). This effect is more pronounced in larger DEX droplets, and may be exploited in the future to, for example, quantify the ultralow interfacial tension of the ATPS solution, by measuring the aspect ratio of the elongated droplets.

Unlike in conventional oil-water systems, in our ultralow interfacial tension system, the shear stress from the fluid flow is able to overcome the tendency of drops to minimize their interfacial area and form spheres. A conventional oil-water emulsion would tend to expand to the sidewalls of the microchannel or form spheres in the microchannel.[40–42] Here, as the drops flow into outlet reservoir, they are no longer under shear stress from the flow, so the drops become spheres (Fig. 4 (b) and Supplementary Information Movie 5).

3.4 Controlling the size ATPS droplets

Figs. 5 (a) and (b) show values of the resulting DEX droplet radius a, plotted against the DEX phase inlet pressure 'on' time t_{on} (Fig. 5 (a)) and 'off' time t_{off} (Fig. 5 (b)). In Fig. 5 (a) the 'off' time $t_{off} = 600$ ms, and in Fig. 5 (b) the 'on' time $t_{on} = 80$ ms. Here, we use four combinations of the DEX phase 'on' pressure $P_o = 21$ or 42 kPa, and PEG phase con-

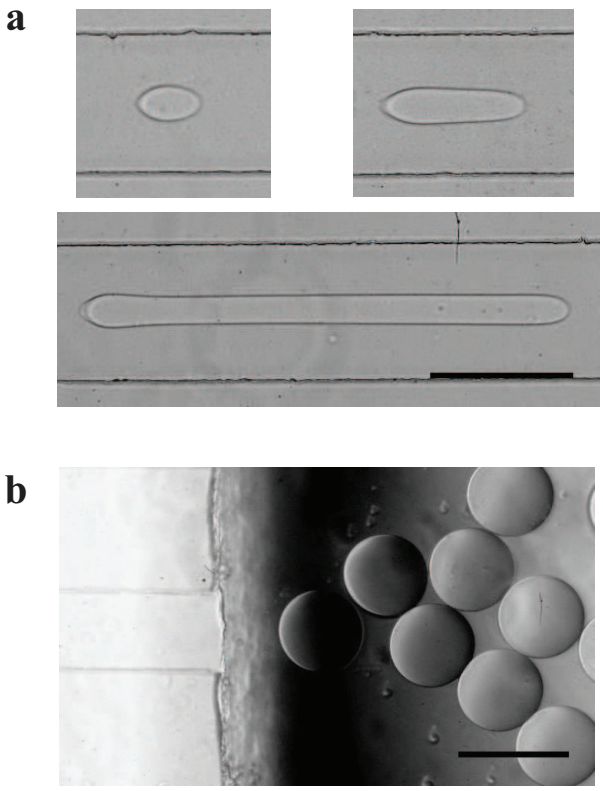

Fig. 4 (a) Different size and shape of droplets downstream in the microchannel. Due to the high capillary number in the flow, the droplets have elongated shapes. (b) The droplets become spheres as they move into the outlet reservoir, where the flow slows dramatically and the drops are no longer confined in the channel. Scale bar 200 μm.

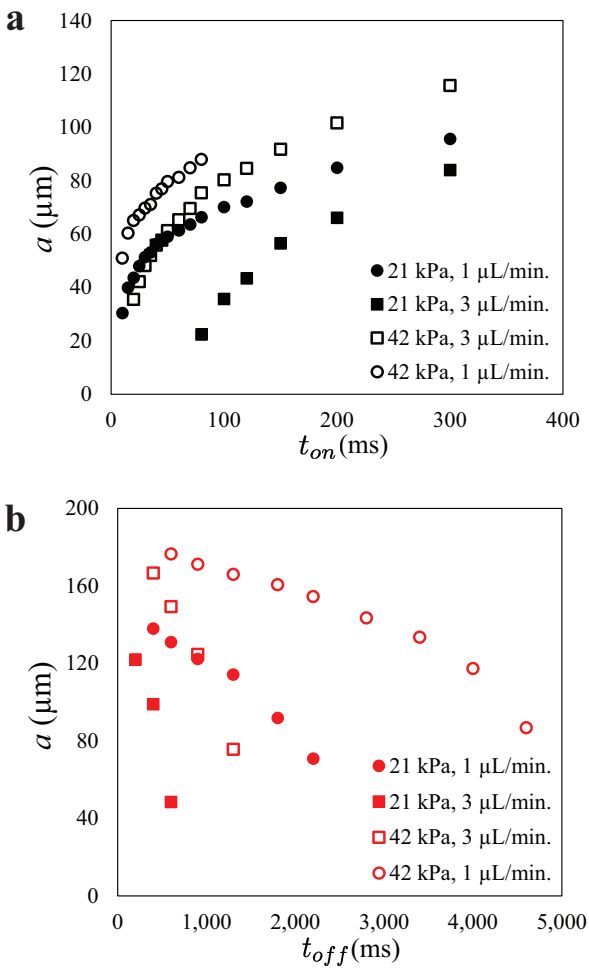

Fig. 5 (Color online) Plots of measured DEX droplet radius a versus the 'on' and 'off' times of the DEX phase inlet pressure. We plot four different combinations of experimental conditions with the applied DEX pressure $P_o = 21$ or 42 kPa, and PEG flow rate $Q_o = 1$ or 3 μL min^{-1}. (a) Drop radius a versus DEX pressure 'on' time t_{on}, while the 'off' time $t_{off} = 600$ ms. (b) Drop radius a versus the DEX phase pressure 'off' time t_{off}, while the 'on' time $t_{on} = 80$ ms.

stant flow rate $Q_o = 1$ or 3 μL min^{-1}, to obtain the experimental results, and we measure the radius of the drops at the microchannel reservoir (Fig. 4 (b)).

The plots (Figs. 5 (a) and (b)) show monotonic increasing droplet radius a with longer DEX phase pressure 'on' times t_{on}, and shorter 'off' times t_{off}. We also note that DEX phase drop radius a grows with higher DEX phase applied pressure P_o, and with lower PEG phase flow rate Q_o. The droplets that we produce range in size from $a = 22$ to 177 μm.

In the limit of higher values of the DEX phase pressure 'on' time (such that the transient ramp-up time of the flow speed can be neglected), we note that the droplet volume is proportional to the product of the resulting DEX phase flow rate Q_D and the 'on' time t_{on}, and inversely proportional to the PEG phase flow rate Q_o and the DEX phase pressure 'off' time t_{off},

$$\left(\frac{a}{w}\right)^3 \propto \frac{Q_D}{Q_o}\frac{t_{on}}{t_{off}}, \tag{1}$$

where, during the time when the DEX phase pressure is applied, the steady-state DEX phase flow rate $Q_D = U\, w\, h$. Here, U is the average speed of the DEX phase. The Hele-Shaw type Stokes flow relationship in the flow (x) direction,

$$\frac{\partial P}{\partial x} \approx \mu_D \frac{\partial^2 u}{\partial y^2}, \tag{2}$$

where u is the flow velocity, and y is the direction normal to the flow along the channel height (Fig. 1 (a)). Eqn. (2) gives the scaling representation of the average flow speed U,

$$U \propto \frac{h^2}{\ell}\frac{P_o}{\mu_D}. \tag{3}$$

Substituting $Q_D = U\, w\, h$ and Eqn. (3) into Eqn. (1), we obtain the scaling relationship for the generated DEX droplet radius,

$$\frac{a}{w} = \kappa\left(\frac{w\,h^3}{\ell}\frac{P_o\, t_{on}}{\mu_D\, Q_o\, t_{off}}\right)^{1/3}, \tag{4}$$

which has the proportionality constant κ.

Eqn. (4) gives the prediction that DEX droplets will be larger with higher values of the applied pressure, P_o, and the time t_{on} over which the pressure is 'on'. The model also indicates that the radius of the droplets will decrease with increasing continuous PEG phase flow rate, Q_o, and the DEX phase pressure 'off' time, t_{off}. All of this is qualitatively consistent with our experimental observations (see for example Figs. 5 (a) and (b)).

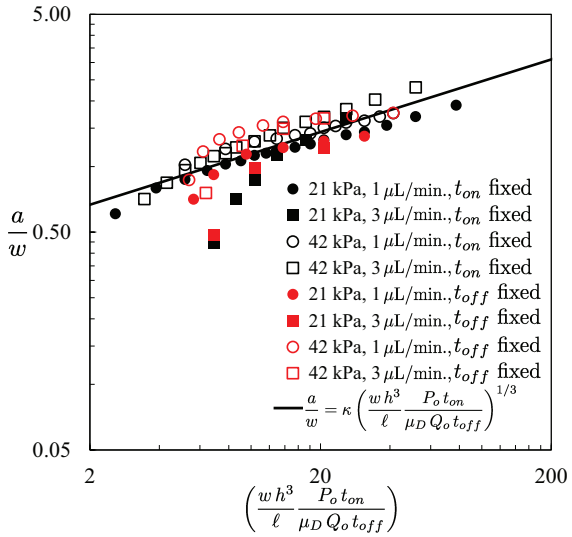

Fig. 6 (Color online) Log-log plot of the ATPS droplet dimensionless radius a/w, versus the dimensionless parameter $wh^3 P_o t_{on}/\ell \mu_D Q_o t_{off}$. Experimental values from eight different combinations of flow conditions are shown, and the results show a good agreement with the scaling model (solid line).

Fig. 6 is a log-log plot of the dimensionless DEX droplet radius a/w versus the dimensionless parameter $wh^3 P_o t_{on}/\ell \mu_D Q_o t_{off}$. All of the experimental results from Figs. 5 (a) and (b) collapses onto a single curve, and display a good quantitative agreement with with our scaling model in Eqn. (4). Namely, the experimental data reflect our predicted 1/3 power-law, and we obtain an empirical value of the proportionality constant $\kappa \approx 0.53$, by fitting our scaling model with the experimental data. The agreement between our model and experiments indicates the utility of the model (Eqn. (4)) for designing future microfluidic ATPS emulsion generation schemes.

3.5 Scaling-up to simultaneous double droplet formation

One limitation of our ATPS droplet generation technique is that the production rate is typically $O(0.1) - O(1)$ droplets per second. This limitation arises because the DEX phase applied pressure 'off' time t_{off} has to be sufficiently long to enable DEX droplets to form (Fig. 2 (a)). However, we may be able to overcome this limitation by scaling-up our droplet production process.

Fig. 7 shows a proof-of-concept scale-up of our microfluidic ATPS droplet generation technique. Here, we take advantage of a parallel flow microfluidic setup,[43–45] to design a multiplexed ATPS droplet generator. We apply a single pressure source, P_o at the DEX phase inlet. With a branched inlet channel design, the DEX phase flows into the flow focusing

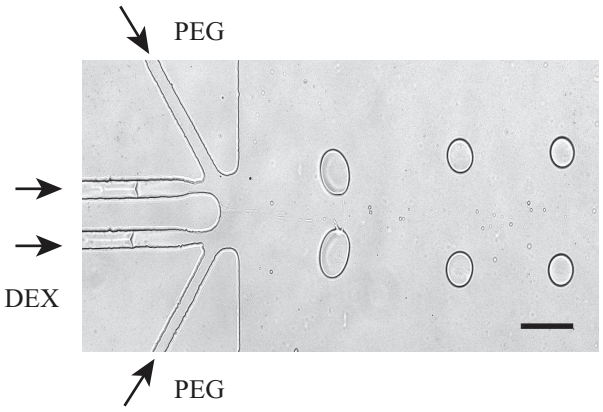

Fig. 7 Image of simultaneous multiple ATPS droplet formation in the microchannel. Two drops are generated at the same time with a single pressure source. Here, the continuous PEG solution (40 % (w/v)) is flowed at 1 μL min^{-1}, and the disperse DEX phase (5 % (w/v)) is injected with an 'on' pressure $P_o = 21$ kPa. Pressure 'on' and 'off' times $t_{on} = 70$ ms and $t_{off} = 600$ ms, respectively. Scale bar 200 μm.

junction from two channels. The continuous phase PEG flows at a constant flow rate Q_o, as before. 5 % (w/v) DEX and 40 % (w/v) PEG are used for this experiment. The DEX phase (5 % (w/v)) is supplied with an 'on' pressure $P_o = 21$ kPa. Pressure 'on' and 'off' times $t_{on} = 70$ ms and $t_{off} = 600$ ms, respectively.

The image in Fig. 7 shows the proof-of-concept of the scaling-up of our method (see also Supplementary Information Movie 6). Since multiplexing of a pressure-driven flow is possible with a parallel flow system, our pressure-assisted ATPS emulsion making technique has the potential to scale-up massively via many parallel disperse phase channels. To demonstrate this approach, a parallel integrated ATPS droplet generator is now under investigation in our group, to more significantly increase the production rate of ATPS droplets. An early prototype of a device that generates 8 ATPS droplets simultaneously is shown in Supplementary Information Fig. S3.

4 Conclusions

We demonstrate a microfluidic ATPS droplet formation system that utilizes a pulsating applied pressure, and hydrodynamic flow focusing. The on-off pressure cycles of the disperse DEX phase, in combination with the constant flow rate continuous PEG phase, make it possible to controllably produce monodisperse ATPS droplets in a flow focusing junction.

We experimentally observe different droplet formation regimes that depend on experimental parameters such as the applied pressure magnitude P_o, the continuous phase flow rate Q_o, and the 'on' and 'off' times of the applied pressure t_{on} and

t_{off}, respectively. We also produce droplets that vary by an order of magnitude in volume, from $O(10)$ pL to $O(10)$ nL, and our simple scaling model captures quantitatively the physics that determine the resulting droplet size. Finally, we show the proof-of-concept of the scaling-up of our ATPS droplet making scheme, by multiplexing the formation of droplets in a parallel-flow system.

Our microfluidic platform offers a simple method to create monodisperse ATPS droplets. This setup overcomes the challenges associated with the ultralow interfacial tension of ATPS, by combining a pulsating disperse phase pressure, and a constant continuous phase flow rate. This method is applicable to on-demand drop formation applications.[46,47] We also anticipate that this approach may have utility in biological applications where the biocompatible nature of ATPS is desirable, for example, in cell encapsulation,[48] particle coating,[49,50] and drug delivery.[51]

5 Acknowledgements

S. S. H. Tsai (grant no. 435514-2013) and D. K. Hwang (grant no. 386092-2010) both acknowledge funding support from the Natural Sciences and Engineering Research Council (NSERC) Discovery grants program. S. G. Jones acknowledges funding support from the Ontario Graduate Scholarships program.

References

1 H. Walter and G. Johansson, *Methods in Enzymology*, Academic Press New York, 1994, vol. 228.
2 J. A. Asenjo and B. A. Andrews, *Journal of Chromatography A*, 2011, **1218**, 8826–8835.
3 P.-Å. Albertsson, *Partition of cell particles and macromolecules*, Wiley New York, 1986, vol. 346.
4 H. Walter, G. Johansson and D. E. Brooks, *Analytical Biochemistry*, 1991, **197**, 1–18.
5 J. C. Merchuk, B. A. Andrews and J. A. Asenjo, *Journal of Chromatography B: Biomedical Sciences and Applications*, 1998, **711**, 285–293.
6 U. Sivars and F. Tjerneld, *Biochimica et Biophysica Acta (BBA)-General Subjects*, 2000, **1474**, 133–146.
7 A. Kumar, M. Kamihira, I. Y. Galaev, B. Mattiasson and S. Iijima, *Biotechnology and Bioengineering*, 2001, **75**, 570–580.
8 M. Yamada, V. Kasim, M. Nakashima, J. Edahiro and M. Seki, *Biotechnology and Bioengineering*, 2004, **88**, 489–494.
9 J. P. Frampton, D. Lai, H. Sriram and S. Takayama, *Biomedical Microdevices*, 2011, **13**, 1043–1051.
10 T. Yaguchi, S. Lee, W. S. Choi, D. Kim, T. Kim, R. J. Mitchell and S. Takayama, *Analyst*, 2010, **135**, 2848–2852.
11 H. Tavana, A. Jovic, B. Mosadegh, Q. Lee, X. Liu, K. Luker, G. Luker, S. Weiss and S. Takayama, *Nature Materials*, 2009, **8**, 736–741.
12 C. Kepka, J. Rhodin, R. Lemmens, F. Tjerneld and P.-E. Gustavsson, *Journal of Chromatography A*, 2004, **1024**, 95–104.
13 A. Azevedo, P. Rosa, I. Ferreira, A. Pisco, J. De Vries, R. Korporaal, T. Visser and M. Aires-Barros, *Separation and Purification Technology*, 2009, **65**, 31–39.
14 H. Song, D. L. Chen and R. F. Ismagilov, *Angewandte Chemie International Edition*, 2006, **45**, 7336–7356.
15 S.-Y. Teh, R. Lin, L.-H. Hung and A. P. Lee, *Lab on a Chip*, 2008, **8**, 198–220.
16 S. Sharma, M. Srisa-Art, S. Scott, A. Asthana and A. Cass, *Microfluidic Diagnostics*, 2013, **949**, 207–230.
17 R. Tewhey, J. B. Warner, M. Nakano, B. Libby, M. Medkova, P. H. David, S. K. Kotsopoulos, M. L. Samuels, J. B. Hutchison, J. W. Larson *et al.*, *Nature Biotechnology*, 2009, **27**, 1025–1031.
18 D. K. Hwang, D. Dendukuri and P. S. Doyle, *Lab on a Chip*, 2008, **8**, 1640–1647.
19 M. T. Guo, A. Rotem, J. A. Heyman and D. A. Weitz, *Lab on a Chip*, 2012, **12**, 2146–2155.
20 L. Mazutis, J. Gilbert, W. L. Ung, D. A. Weitz, A. D. Griffiths and J. A. Heyman, *Nature Protocols*, 2013, **8**, 870–891.
21 S. Hardt and T. Hahn, *Lab on a Chip*, 2012, **12**, 434–442.
22 R. J. Meagher, Y. K. Light and A. K. Singh, *Lab on a Chip*, 2008, **8**, 527–532.
23 J. R. SooHoo and G. M. Walker, *Biomedical Microdevices*, 2009, **11**, 323–329.
24 K. Vijayakumar, S. Gulati and J. B. Edel, *Chemical Science*, 2010, **1**, 447–452.
25 R. Hatti-Kaul, *Molecular Biotechnology*, 2001, **19**, 269–277.
26 E. Atefi, J. A. Mann Jr and H. Tavana, *Langmuir*, 2014, **30**, 9691–9699.
27 S. D. Geschiere, I. Ziemecka, V. van Steijn, G. J. Koper, J. H. van Esch and M. T. Kreutzer, *Biomicrofluidics*, 2012, **6**, 022007.
28 Y. S. Song, Y. H. Choi and D. H. Kim, *Journal of Chromatography A*, 2007, **1162**, 180–186.
29 Y. H. Choi, Y. S. Song and D. H. Kim, *Journal of Chromatography A*, 2010, **1217**, 3723–3728.
30 I. Ziemecka, V. van Steijn, G. J. Koper, M. Rosso, A. M. Brizard, J. H. van Esch and M. T. Kreutzer, *Lab on a Chip*, 2011, **11**, 620–624.
31 I. Ziemecka, V. van Steijn, G. J. Koper, M. T. Kreutzer and J. H. van Esch, *Soft Matter*, 2011, **7**, 9878–9880.
32 D. Lai, J. P. Frampton, H. Sriram and S. Takayama, *Lab on a Chip*, 2011, **11**, 3551–3554.
33 H. C. Shum, J. Varnell and D. A. Weitz, *Biomicrofluidics*, 2012, **6**, 012808.
34 A. Sauret and H. C. Shum, *Applied Physics Letters*, 2012, **100**, 154106.
35 Y. Song and H. C. Shum, *Langmuir*, 2012, **28**, 12054–12059.
36 H. Tavana, B. Mosadegh and S. Takayama, *Advanced Materials*, 2010, **22**, 2628–2631.
37 D. Forciniti, C. Hall and M. Kula, *Journal of Biotechnology*, 1990, **16**, 279–296.
38 Y. Xia and G. M. Whitesides, *Annual Review of Materials Science*, 1998, **28**, 153–184.
39 D. Dendukuri, S. S. Gu, D. C. Pregibon, T. A. Hatton and P. S. Doyle, *Lab on a Chip*, 2007, **7**, 818–828.
40 D. M. Fries, F. Trachsel and P. R. von Rohr, *International Journal of Multiphase Flow*, 2008, **34**, 1108–1118.
41 L. Shui, A. van den Berg and J. C. Eijkel, *Journal of Applied Physics*, 2009, **106**, 124305.
42 M. Grad, C. Tsai, M. Yu, D. Kwong, C. Wong and D. Attinger, *Measurement Science and Technology*, 2010, **21**, 075204.
43 T. Thorsen, S. J. Maerkl and S. R. Quake, *Science*, 2002, **298**, 580–584.
44 W. Li, E. W. K. Young, M. Seo, Z. Nie, P. Garstecki, C. A. Simmons and E. Kumacheva, *Soft Matter*, 2008, **4**, 258–262.
45 B.-U. Moon, S. S. Tsai and D. K. Hwang, *Microfluidics and Nanofluidics*, 2015, DOI: 10.1007/s10404–015–1548–6.
46 H. Dong, W. W. Carr and J. F. Morris, *Physics of Fluids (1994-present)*, 2006, **18**, 072102.
47 J.-C. Galas, D. Bartolo and V. Studer, *New Journal of Physics*, 2009, **11**,

075027.
48 G. Orive, R. M. Hernández, A. R. Gascón, R. Calafiore, T. M. Chang, P. De Vos, G. Hortelano, D. Hunkeler, I. Lacík, A. J. Shapiro and J. L. Pedraz, *Nature Medicine*, 2003, **9**, 104–107.
49 S. S. Tsai, J. S. Wexler, J. Wan and H. A. Stone, *Applied Physics Letters*, 2011, **99**, 153509.
50 B.-U. Moon, N. Hakimi, D. K. Hwang and S. S. Tsai, *Biomicrofluidics*, 2014, **8**, 052103.
51 C. Berkland, K. K. Kim and D. W. Pack, *Journal of Controlled Release*, 2001, **73**, 59–74.